U.S. DEPARTMENT OF THE INTERIOR

U.S. GEOLOGICAL SURVEY

CALIBRATION OF THE "GAS EFFECT" USING NEUTRON, DENSITY, AND GAMMA-RAY-INTENSITY WIRE-LINE LOGS

by

Timothy C. Hester[1]

Open-File Report 99-128

[1]U.S. Geological Survey, Box 25046, MS 939, Lakewood, CO 80225

1999

CONTENTS

ILLUSTRATIONS

INTRODUCTION

Unconventional (tight), clay-rich reservoirs are not well suited to conventional methods of formation evaluation (Kowalchuk et al, 1974; Whitney and Ahlbrandt, 1996). Potential pay zones are often poorly defined on geophysical well logs and thus overlooked. Both shallow and deep reservoirs from similar depositional environments may be equally difficult to evaluate, but with the additional economic constraints associated with deep reservoirs, risk is increased. An easy-to-use calibration developed here quantifies the "gas effect" (the response of neutron- and density-porosity tools to the presence of gas) with respect to actual production and simplifies the identification and selection of potential gas-producing intervals at any depth. Geologic factors targeted by conventional log analyses, such as effective porosity, clay content, and water saturation, although strongly affected by burial, compaction, thermal maturation, and diagenesis, are combined and accounted for empirically using a single "gas-production index" (GPI). GPI, introduced here for the first time, in effect, links log-derived, in-situ rock properties with production potential. The fundamental mechanism for isolating the gas effect for calibration is the neutron porosity minus density porosity (N-D) vs gamma-ray intensity (GRI) crossplot, which was introduced in the early 1970s with the commercial availability of the compensated neutron and density wireline logging tools.

The relation of neutron, density, and gamma-ray tool responses to the presence of clay and gas in a formation is expressed graphically (Fig. 1) by plotting the difference between neutron and density porosity (N-D, y-axis) against gamma-ray intensity (GRI, x-axis). This method has been used in the past to distinguish gas-producing from water-producing intervals in very shaly formations where conventional log-analyses are ineffective. The inventor of this crossplot and specifically how it came into popular use is not in the published literature. Case histories presented in Cutress (1974) document the utility of the crossplot as a gas-detection tool in the Viking formation of east-central Alberta, Canada, and in Campen (1975) numerous formations in the Cretaceous biogenic gas sands of northern Montana. These shallow biogenic sandstones are used as an example in this report to test the method, which will be later applied to sandstones in general, including deep sandstones of the Anadarko basin.

Effectiveness of the crossplot (Fig. 1) depends on the existence, close proximity, and identification of water-saturated zones with geologic and production characteristics similar to those of prospective gas-producing intervals. Log measurements from the water-saturated zones are plotted to establish a "liquid line" (Cutress, 1974; Campen, 1975), which then serves to separate gas-producing from water-producing (or non-producing) intervals. Gas-bearing zones with production potential plot below the liquid line. The departure of the gas-bearing zones from the liquid line is the "gas effect", a term that refers to the well known opposing response of neutron- and density-porosity curves to the presence of gas in the formation. Typically, a liquid line is constructed for each formation of interest in a local area. The ideal position of the liquid line is often difficult to establish, and may vary depending upon porosity, the degree of water saturation, and economic or production criteria specific to the formation or operator. Figure 1 shows a schematic N-D vs GRI crossplot with hypothetical liquid line and producing-interval data.

In continuous-type (unconventional; Schmoker, 1995) gas accumulations of the northern Great Plains, and perhaps in other regions with similar depositional environments, 100 percent water-saturated zones are relatively uncommon. In addition, existing water sands are not always adjacent to prospective production, similar in clay content, or easily recognizable on well logs. Regional studies over broad geographic areas or investigations involving multiple formations are additionally complicated by the difficulties in constructing and interpreting multiple liquid lines.

A simple, more robust, system of gas detection in shaly sands is developed here. The new system uses the same crossplot, but eliminates the need to construct liquid lines for each formation, allowing formations with varying geologic characteristics to be compared at the same time. In addition, the systematic functioning of the crossplot (detailed in a following section) allows the plotted distribution of gas-bearing intervals to be explained in terms of relative variation in porosity and water saturation, clay content, bound water, and production potential. Thus, the crossplot becomes an interpretive tool in support of (or in lieu of) conventional formation evaluation.

This report reviews geophysical tool response to clay and gas. The two crossplotted variables N-D and GRI are discussed in terms of porosity using the dual water model (Fig. 2) modified from that shown schematically in Schlumberger (1987). A series of generalized equations is used to establish a conceptual link among tool response, porosity, and the two crossplotted variables. Finally, the calibration of the gas effect is explained, and integrated with some geologic interpretations.

An important part of developing this method for a broader application is to develop a link between the gas effect and production potential for wells at different depths. Cretaceous reservoirs of the northern Great Plains are used here to test the method and establish a lower limit for production potential. Deep, high-cost wells are economically viable only at higher production rates. Additional data from deep gas-producing wells will be necessary to determine the upper limit of the production range.

This report was funded in part by the Gas Research Institute, Chicago, Illinois (through a Cooperative Research and Development Agreement with Advanced Resources International, Arlington, Virginia), the U.S. Department of Energy (contract no. DE-AT26-98FT40032), Morgantown, West Virginia, and the Energy Resources Program of the U.S. Geological Survey, Denver, Colorado.

GAMMA RAY, NEUTRON, AND DENSITY TOOL RESPONSE

The relation of gamma ray, neutron and density tool response is effective in accounting for clay, porosity, and water saturation empirically, and for isolating the gas effect in a useful and predictable way. Understanding the relation is an important part of linking the N-D vs GRI crossplot with geology, calibrating the gas effect, and developing the crossplot as an analysis tool for making basic interpretations of the data. To that end, tool response to clay and gas, and the crossplotted variables N-D and GRI are explained and linked with the dual water model using a series of generalized equations. The term "effective" porosity includes free (movable) water and hydrocarbons, "total" porosity includes effective porosity and clay-bound (immovable) water (Fig. 2).

Effect of Clay

Heslop (1974) showed that GRI in shaly sandstones increases linearly with clay volume. Clay volume is measured independent of "shale" volume using relative gamma-ray deflections (percent) converted to API units. Clay volume is important because of its effect on porosity, permeability, and geophysical tool response. Because his GRI data were limited to about 100 API, Heslop was unable to establish an upper limit for his linear trend; he therefore suggested that his clay-volume estimates were probably high (Heslop, 1974). The data set presented here includes GRI values as high as 175 API for intervals in the Cretaceous Bowdoin sandstone, where core and log data indicate clay content up to 50 percent (Henry, 1979; Kukal, 1981). Using these new data as an upper endpoint, and applying Heslop's linear trend, a scale for estimated clay volume is shown opposite the GRI axis for Figures 3 through 7, and 9. This scale does not account for varying proportions of clay minerals with different intrinsic radioactivity levels.

Clay volume estimated in this way is a rough approximation, used here only for comparison and to investigate regional trends. As clay volume increases, bound water also increases. A linear relation of bound water with clay volume is demonstrated in the next section. The following paragraphs outline the response of neutron- and density-porosity tools to the presence of clay and associated bound water.

The neutron tool responds primarily to hydrogen in the formation (Schlumberger, 1987). Hydrogen is a major component of saturating pore fluids (free water and hydrocarbons) and bound water associated with clay, but may also be present in clay minerals in the form of hydroxyl ions (-OH) or in non-porous hydrous minerals such as gypsum in the form of chemically attached water of crystallization (Schlumberger, 1987). Under normal circumstances and in many clean producing formations, saturating pore fluids contribute overwhelmingly to the amount of hydrogen per unit volume (hydrogen index). Thus, in most conventional liquid-filled reservoirs, the neutron tool measures total porosity. The generalized equation,

$$\emptyset_{NEUTRON} = \emptyset_{BW} + \emptyset_{FW} + \emptyset_{HC} = \emptyset_{TOTAL} \qquad (1)$$

where $\emptyset_{BW}$ is porosity due to bound water, $\emptyset_{FW}$ is porosity due to free water, and $\emptyset_{HC}$ is porosity due to hydrocarbons, reflects the response of the neutron tool to liquid-filled porosity in terms of the dual water model (Fig. 2).

The density tool responds primarily to electron density, which varies with formation bulk density (Schlumberger, 1987). Bulk-density measurements incorporate all formation constituents including both solid and fluid components. Porosity is determined algebraically by assigning values for matrix and fluid density. In formations where lithology and fluid type are well known (and therefore matrix- and fluid-density values are correct) the density tool provides a reliable measure of effective porosity. The generalized equation,

$$\emptyset_{DENSITY} = \emptyset_{FW} + \emptyset_{HC} = \emptyset_{EFFECTIVE} \qquad (2)$$

reflects the response of the density tool in terms of the dual water model (Fig. 2).

In formations with liquid-filled porosity (under ideal conditions, using correct matrix and fluid densities), the crossplotted variable N-D (y-axis, Fig. 1) empirically accounts for effective porosity (subtracting equations 1 and 2, and combining terms),

$$N\text{-}D = \phi_{NEUTRON} - \phi_{DENSITY} = (\phi_{BW} + \phi_{FW} + \phi_{HC}) - (\phi_{FW} + \phi_{HC})$$

$$= \phi_{BW} \qquad (3)$$

and thus, reflects porosity associated with bound water.

Effect of Gas

The hydrogen index of liquid hydrocarbons is nearly that of water (Schlumberger, 1987). Therefore, the neutron tool measures total porosity in either oil or water-filled formations. Gas, however, contains much less hydrogen than water or liquid hydrocarbons and causes the neutron tool to measure porosity too low. In addition, the excavation effect (Segesman and Liu, 1971) causes the neutron tool to measure porosity even lower than that accounted for by the reduction in hydrogen index. The excavation effect is enhanced in combination with water (saturating or bound) and maximized at higher porosities, intermediate water saturations, and (or) higher clay volumes. Correcting equation 1 for gas using the term $-(\phi_g + \phi_{EX})$, equation 4 becomes,

$$\phi_{NEUTRON} = \phi_{BW} + \phi_{FW} + \phi_{HC} - (\phi_g + \phi_{EX}) \qquad (4)$$

where, ϕ_g and ϕ_{EX} are porosity due to gas and the excavation effect, respectively. The minus sign reflects a negative contribution to the porosity measurement of the neutron tool due to the presence of gas. Thus, neutron porosity in the presence of gas is a measure of total porosity minus the effect of gas and excavation.

When neutron porosity is plotted against clay content, the effects of bound water become apparent. The regression line of Figure 3, a plot of neutron porosity vs GRI (a measure of clay content) for all gas-producing intervals of the data set, shows a systematic, linear increase in neutron porosity as clay content (GRI) increases. Neutron porosity increases as hydrogen associated with clay-bound water increases. In gas-charged formations, such as those represented by the data of Figure 3, bound water is the primary contributor to the hydrogen index. Thus, the sample coefficient of determination ($r^2 = 0.66$) indicates that about two-thirds of the change in the neutron response is due to the linear increase of bound water associated with increasing clay content. Data scatter about the regression line reflects variations in effective porosity and gas saturation.

The density of oil and water are similar compared to that of natural gas, which is much lower. In the presence of gas, the density tool measures a lower bulk density (and calculates a higher porosity), more or less proportional to the percent volume of gas present. Adding the term $\emptyset_G$ to equation 2, equation 5 becomes,

$$\emptyset_{DENSITY} = \emptyset_{FW} + \emptyset_{HC} + \emptyset_G \qquad (5)$$

where $\emptyset_G$ is the addition of apparent porosity to the density tool measurement as a result of gas in the formation. Without adjustment to the fluid-density value to account for the lower density of the gas, calculated effective porosity will be too high, reflecting the measurement of effective porosity plus gas porosity.

In formations with gas-charged effective porosity, the variable N-D can be written (subtracting equations 4 and 5 and combining terms) as equation 6.

$$\begin{aligned} N\text{-}D = \emptyset_{NEUTRON} - \emptyset_{DENSITY} &= (\emptyset_{BW} + \emptyset_{FW} + \emptyset_{HC} - \emptyset_g - \emptyset_{EX}) - (\emptyset_{FW} + \emptyset_{HC} + \emptyset_G) \\ &= \emptyset_{BW} + \emptyset_{FW} + \emptyset_{HC} - \emptyset_g - \emptyset_{EX} - \emptyset_{FW} - \emptyset_{HC} - \emptyset_G \\ &= \emptyset_{BW} - \emptyset_g - \emptyset_{EX} - \emptyset_G \\ &= \emptyset_{BW} - (\emptyset_g + \emptyset_{EX} + \emptyset_G) \qquad (6) \end{aligned}$$

When the variable N-D is plotted against GRI (Fig. 4), bound water ($\emptyset_{BW}$; equation 6) is empirically accounted for as a function of clay content, and vertical variation of the plotted data becomes a measure of the cumulative gas effect: $-(\emptyset_g + \emptyset_{EX} + \emptyset_G)$. The negative value reflects displacement below the liquid line (e.g., Fig. 1).

CALIBRATION OF THE GAS EFFECT

The algebraic difference between neutron and density porosity (N-D, y-axis) in liquid-filled formations is a measure of bound water (equation 3). In the presence of gas, N-D is a measure of bound water minus the gas effect (equation 6). When N-D is plotted against clay volume (GRI), the effects of bound water and gas are separated. Figure 4 shows all gas-producing intervals of this report plotted on the N-D vs GRI crossplot. The least-squares regression line shows the dependence of N-D on gamma-ray intensity. Clay content (Heslop, 1974) and bound water increase linearly with gamma-ray intensity. Thus, the sample coefficient of determination ($r^2 = 0.58$) indicates that more than half of the change in N-D is due to variation in clay content and associated bound water. Data scatter about the regression line is due to variation in the gas effect.

The term "gas effect" refers to the opposing response of neutron- and density-porosity curves to the presence of gas in the formation. Some scatter, not related to in-situ gas volume, is introduced by differing tool responses to porosity and by the irregular enhancement of excavation (equation 4) as porosity, water saturation, and clay content and mineralogy vary (Segesman and Liu, 1971). Therefore, the magnitude of the gas effect (equation 6) is closely, but not precisely, related to the absolute in-situ volume of gas measured by the combination of the two porosity tools. This variation is not easily quantified and thus imposes a limit on the degree of resolution possible for the gas effect. An intermediate index—"GPI" (gas-production index), is introduced here to smooth that variation and to link the gas effect to production potential. Note the subtle but important conceptual difference between the "gas effect"—a tool response to a given volume of in-situ gas, and "GPI"—a measure of the gas effect, with respect to actual production.

The calibration system using GPI consists of two fundamental components: 1) a baseline from which the gas effect can be measured (e.g., a liquid line, Fig. 1); and 2) an incremental system that maximizes resolution of the gas effect within the limits prescribed by the otherwise unaccounted-for variations in tool response and excavation. In this system, no water-bearing intervals or liquid lines as such are used. Instead, a "zero-production baseline" is empirically determined using 242 producing intervals from 53 wells of the production data set. This baseline represents the cutoff of commercial gas production. In this way, the limits of the data empirically define the ultimate limits of gas production for an entire region or several regions. This baseline is the cornerstone of the calibration system, which allows intervals or formations within a well, or from different wells, to be compared with each other in the context of production potential.

Calibration System

The calibration system (Fig. 5) consists of 2 sets of parallel lines positioned on the crossplot to conform to 3 fundamental ideas: 1) the absence of producing-interval data represents a theoretical "zero" production potential, therefore, line segments bounding the data ultimately define the limits of gas production for the region; 2) the gas effect increases vertically downward from these line segments in a systematic and predictable way; and 3) there is a definable clay volume, above which, gas-production rapidly declines.

Two heavy line segments bound the data of Figure 5 (all gas-producing intervals) —a diagonal line and a horizontal line. Both are hand drawn to include the maximum number of data points (about 98 percent) and to minimize outliers. Straight-line segments are used (both diagonally and horizontally) because they better constrain the data throughout the range of GRI than do curved lines. The slopes and point of intersection of these line segments (where GRI=100 API) are artifacts of an empirical "best fit" to the data. Together, these line segments establish a regional "liquid line" (without using water-bearing intervals) for all producing formations. Shallow Cretaceous

reservoirs of northern Montana are used here as a test group to approximate the economic lower limit, or "cutoff", of commercial gas production. This economic cutoff is represented on the chart by the two heavy line segments, and is referred to as the "zero-production baseline". All other lines are parallel to these. Intervals that plot above this baseline are unlikely to deliver commercial volumes of gas. Deep gas reservoirs, usually hotter and drier than those of the northern Great Plains, may also fit within these criteria.

Below the baseline, gas production without water is not guaranteed, but the potential increases with decreasing N-D (Fig. 5). The magnitude of displacement is measured using a series of lines parallel to the empirically-defined zero-production baseline. These lines (separate and distinct from the baseline) envelope and subdivide the data, and scale the gas effect into 12 levels of GPI (Fig. 5). The levels are equally spaced in the vertical direction and numbered consecutively, increasing from top to bottom (the 12^{th} level is open-ended). Thus, GPI increases linearly as a function of the level occupied by a data point. This linear index reflects an assumed linear relation of the gas effect to in-situ gas volume. This is not precisely the case, however, because the excavation effect (equation 4) varies in a non-linear way as geologic conditions change. Thus, the cumulative gas effect (equation 6) may vary somewhat with factors other than the volume of gas present. The average excavation effect for sandstone with 20 percent porosity (the approximate average for production-interval data of this report, Fig. 6) may vary as much as 3 percent (Segesman and Liu, 1971). To account for this variation, allow for maximum resolution of the gas effect, and preserve the simplicity of the calibration system, GPI levels span 3 percent porosity.

The slope break for the parallel lines in Figure 5 (80 API) represents the point at which increasing clay volume begins to rapidly degrade reservoir quality. This interpretation (discussed in the following section) is determined by the porosity and production data of this report, and the porosity and clay content data of Schmoker (1997). Using the GPI levels, as opposed to using porosity units of the y-axis (N-D), normalizes the gas effect with respect to the zero-production baseline. This approach allows intervals or formations to be compared with each other without regard to clay content.

THE EFFECT OF CLAY ON POROSITY AND GAS PRODUCTION

Heslop (1974) shows that GRI in shaly sandstones increases linearly with clay volume. Clay volume (as opposed to "shale" volume) is estimated using relative gamma-ray deflections (percent) and converted to API units. Important in Heslop's correlation is a distinction between grain- and matrix-supported lithologies (sand and shale, respectively) and the position of the transition between them. In nature, the transition between these two endpoints is continuous. Here, the transition is represented by a fixed clay volume, marked on the N-D vs GRI crossplot by the intersection of diagonal and horizontal lines (Fig. 5; 80 API). The position of the transition on the crossplot separates the producing formations of this report by age, depositional environment, and reservoir characteristics, and marks the onset of a rapid decline in porosity and gas production. In addition, 80 API separates apparent positive and negative influences of clay on reservoir character.

Generally, the effects of clay on porosity and gas production are negative, reducing overall porosity and permeability by occupying pores, filling pore networks by deforming during burial (Schmoker, 1997), and destroying permeability by expanding and mobilizing during production. In some cases, however, clay appears to be somewhat beneficial to both porosity and production. If permeability is not seriously degraded, some clay (or clay types) might actually "bind" water that would otherwise be produced, and in moderate amounts can preserve porosity (and perhaps permeability) by retarding quartz cementation (Schmoker, 1997).

Schmoker (1997, his Fig. 5) shows that higher porosity (normalized for the level of thermal maturity) in the Lower Cretaceous J sandstone (Dakota Group) of the Denver basin, Colorado, is associated with intermediate clay content (about 12 percent), and that porosity declines as clay content increases or decreases from intermediate values. The data of this report indicate a similar porosity trend and show that gas production in the northern Great Plains is tightly linked to both porosity and clay content.

Compensated density porosity (Fig. 6) and volume of production in the peak calendar year (Fig. 7) are both plotted against clay volume (GRI). Among other trends, the two figures show that porosity and gas production co-vary with clay content. Both variables increase from lower levels to peak at about 60 API, a clay volume consistent with that of the highest porosity values of Schmoker (1997)—roughly 12 percent. Above about 17 percent clay, the suggested transition point between grain- and matrix-supported lithologies (Fig. 5; 80 API), maximum porosity and production decline rapidly. Thus, the optimum clay content for higher porosity in the J sandstone, as suggested by Schmoker (1997), also appears to be the optimum clay content for maximum porosity and gas production in Cretaceous reservoirs of the northern Great Plains, and may range from roughly 7 to 17 percent clay (50 to 80 API). Schmoker's data also show that porosity may be more rapidly reduced by increasing clay volume than by increasing thermal maturation. Therefore, at a given level of thermal maturity, clay content measurements may provide an additional level of detail for porosity prediction, above that of using thermal maturation alone (Schmoker and Hester, 1990).

Clay-rich, low-permeability sandstones (or siltstones) generally have low effective porosity. In contrast, producing intervals tend to be those that retain higher-than-normal porosity as thermal maturity (Hester, 1997) and (or) clay volume increases. The data of Figure 6 show that for gas-producing intervals of this report, overall porosity decline with increasing clay content is negligible ($r^2 = 0.03$). The lack of porosities below 8 percent reflects the economic and geologic bias of the producing-interval data, and suggests that effective porosities of less than 8 percent are probably inadequate for commercial gas production regardless of clay content. As the transition from grain-supported to matrix-supported lithology advances and clay volume exceeds about 35 percent (130 API), the minimum effective porosity required for gas production increases rapidly. As a result, the number of potential producing intervals declines significantly (Fig. 6). The data of Figures 6 and 7, in conjunction with those of Schmoker (1997), suggest that gas production from intervals where clay content exceeds 50 percent (175 API) is rare.

The potential for gas production can be assessed using the N-D vs GRI crossplot and the resulting GPI (Fig. 5). GPI empirically combines porosity, water saturation, and clay content into a single parameter that associates the in-situ rock with the potential to produce gas. GPI may be favorably compared with direct well testing methods such as absolute open flow potential (AOF). AOF was used to evaluate individual well productivity for the Eagle Sandstone of the Cedar Creek anticline, southeast Montana (Green, 1997). AOF was calculated after all perforated intervals were stimulated and a final flow test was conducted. A strong correlation ($r^2 = 0.88$) of AOF with best 12-month cumulative gas production (Green, 1997, his Fig. 5) suggests that AOF testing in this way can be a good indicator of longer term well performance in the Eagle Sandstone. By comparison, using a similar measure of cumulative gas production (Fig. 8, $r^2 = 0.61$), GPI also appears to be a good indicator of longer-term well performance.

Figure 8 shows volume of production in the peak calendar year plotted against GPI, for each of 28 gas-producing wells of this report. GPI for each well is an average of its constituent intervals (Figs. 3-6). The sample coefficient of determination ($r^2 = 0.61$) shows a strong dependence of gas production on GPI. Geologic variables not directly measured by porosity and gamma-ray logs, such as the presence and distribution of natural fractures and clay composition, are accounted for empirically using the zero-production baseline (Fig. 5), and are manifested as scatter about the regression line of Figure 8. The potential for production is shown by the range (dashed lines) associated with a given level of GPI. To the extent that the data are representative of the geology and productivity of the northern Great Plains, Figure 8 reflects typical production rates reasonably expected for a given quality of reservoir rock or producing interval, as measured by GPI. Deep reservoirs are far more expensive to drill and complete than shallow reservoirs and thus have rigid economic constraints requiring significantly higher production rates. Additional data from deeper wells may show a steepened production-rate curve at the high end of the GPI range.

SUMMARY

The potential exists for large volumes of biogenic methane within only a few thousand feet of the surface in the northern Great Plains of the United States. In these shallow wells, production costs are generally low. Nevertheless, limited areas have been exploited and vast areas remain undeveloped. The primary reasons for the lack of development are low production rates (Schmoker, 1995), and the difficulty in recognizing and evaluating gas-charged reservoirs (Rice and Spencer, 1995). Unconventional, continuous-type, gas-charged lithologies, such as those in the northern Great Plains, are often poorly defined on geophysical well logs and not well suited to conventional methods of formation evaluation. Potential producing intervals are frequently overlooked. Deep targets fit the same geophysical criteria but high drilling costs necessitate significantly higher production rates to be economical. The most clay-rich reservoirs, often commercially viable in shallow plays, will necessarily be bypassed in deep reservoirs.

An easy-to-use calibration system developed here (Fig. 5) simplifies identification, evaluation, and selection of potential gas-producing intervals in the varying geologic settings of the Cretaceous of the northern Great Plains and other regions. Geologic parameters targeted by conventional log analyses, such as effective porosity, water saturation, and clay content, are accounted for empirically using a single gas-production index (GPI), that links the gas effect directly with production. Intervals from different formations (or wells) can be compared with each other, on the same plot, in the context of production potential and geologic variation. Figure 9 summarizes and illustrates the influence of variations in porosity and water saturation, clay volume, bound water, and the gas effect, on the relative positions of plotted data.

Intervals that plot below the zero-production baseline (Fig. 5) have a higher potential to produce gas than those that do not. The potential for production increases as N-D (y-axis, Fig. 5) decreases. Geologic and engineering factors, however, such as natural fractures and well-completion techniques, can significantly influence well productivity. Data from Campen (1975) indicate that in Cretaceous reservoirs of the northern Great Plains some water production can occur at GPI levels as high as 7, and in many areas of north-central Montana the success ratio (Schmoker,1995) for gas wells is projected to be as low as 50 percent (Rice and Spencer, 1995). In deep gas reservoirs, completion techniques and success ratios may vary, and the high end of the GPI scale may steepen to reflect higher production rates. The crossplot method described in this report is a robust indicator of gas-production potential, and an interpretative tool that should be considered in conjunction with (or in lieu of) conventional formation evaluation.

REFERENCES CITED

Campen, E. B., 1975, Well log analysis in the Cretaceous gas sands of northern Montana, *in* Energy Resources of Montana: Montana Geological Society 22nd Annual Publication, p. 15-25.

Cutress, W. G., 1974, An empirical approach to log interpretation in the Viking sand of east central Alberta: Society of Professional Well Log Analysts Fifteenth Annual Logging Symposium Transactions, p. G1-17.

Green, T., 1997, Shallow gas completions benefit from advanced stimulation technology: Gas Research Institute, Gas TIPS, Winter 1996/1997, p.14-19.

Henry, K. C., 1979, Gas detection in the extremely shaly Bowdoin Formation of northern Montana: Society of Professional Well Log Analysts Twentieth Annual Logging Symposium Transactions, p. T1-9.

Heslop, A., 1974, Gamma-ray log response of shaly sandstones: Society of Professional Well Log Analysts Fifteenth Annual Logging Symposium Transactions, p. M1-11.

Hester, T.C., 1997, Porosity trends of Pennsylvanian sandstones with respect to thermal maturity and thermal regimes in the Anadarko Basin, Oklahoma, *in* T.S. Dyman, D.D. Rice, and W.A. Westcott, eds., Geologic Controls of Natural Gas in Deep Sedimentary Basins in the United States: United States Geological Survey Bulletin 2146-I, p.105-124.

Kowalchuk, H., G. Coates, and L. Wells, 1974, The evaluation of very shaly formations in Canada using a systematic approach: Society of Professional Well Log Analysts Fifteenth Annual Logging Symposium Transactions, p. H1-21.

Kukal, G.C., 1981, Formation evaluation and gas detection in shallow, low-permeability, shaly sands, of the northern Great Plains province: Journal of Petroleum Technology, v. 33, no. 10, p. 1976-1984.

Rice, D.D., and C.W. Spencer, 1995, Northern Great Plains shallow biogenic gas, *in* Gautier, D.L., Dolton, G.L., Takahashi, K.I., and Varnes, K.L., eds., 1995 National Assessment of United States Oil and Gas Resources—Results, Methodology, and Supporting Data: United States Geological Survey Digital Data Series DDS-30 [CD-ROM].

Schlumberger, 1987, Log Interpretation Principles/Applications (2d ed.): Houston, TX, Schlumberger Educational Services, 198 p.

Schmoker, J.W., 1995, Method for assessing continuous-type (unconventional) hydrocarbon accumulations, *in* D.L. Gautier, G.L. Dolton, K.I. Takahashi, and K.L. Varnes, eds., 1995 National Assessment of United States Oil and Gas Resources—

Results, Methodology, and Supporting Data: United States Geological Survey Digital Data Series DDS-30 [CD-ROM].

Schmoker, J.W., 1997, Porosity predictions in deeply buried sandstones, with examples from Cretaceous formations of the Rocky Mountain region, *in* T.S. Dyman, D.D. Rice, and W.A. Westcott, eds., Geologic Controls of Natural Gas in Deep Sedimentary Basins in the United States: United States Geological Survey Bulletin 2146-H, p.77-104.

Schmoker, J.W., and T.C. Hester, 1990, Regional trends of sandstone porosity vs vitrinite reflectance—A preliminary framework, *in* V.F. Nuccio, and C.E. Barker, eds., Applications of thermal maturity studies to energy exploration: Rocky Mountain Section, Society of Economic Paleontologists and Mineralogists, p. 53-60.

Segesman, F., and O. Liu, 1971, The excavation effect: Society of Professional Well Log Analysts Twelfth Annual Logging Symposium Transactions, p. H1-21.

Whitney, G., and T. S. Ahlbrandt, 1996, Effects of clays on resistivities of clastic rocks and reservoir performance: *in* E.D. Dolly, and J.C. Mullarkey, eds., Hydrocarbon production from low contrast, low resistivity reservoirs Rocky Mountain and Mid-Continent Regions log examples of subtle pays, Rocky Mountain Association of Geologists Guidebook, p. 43-52.

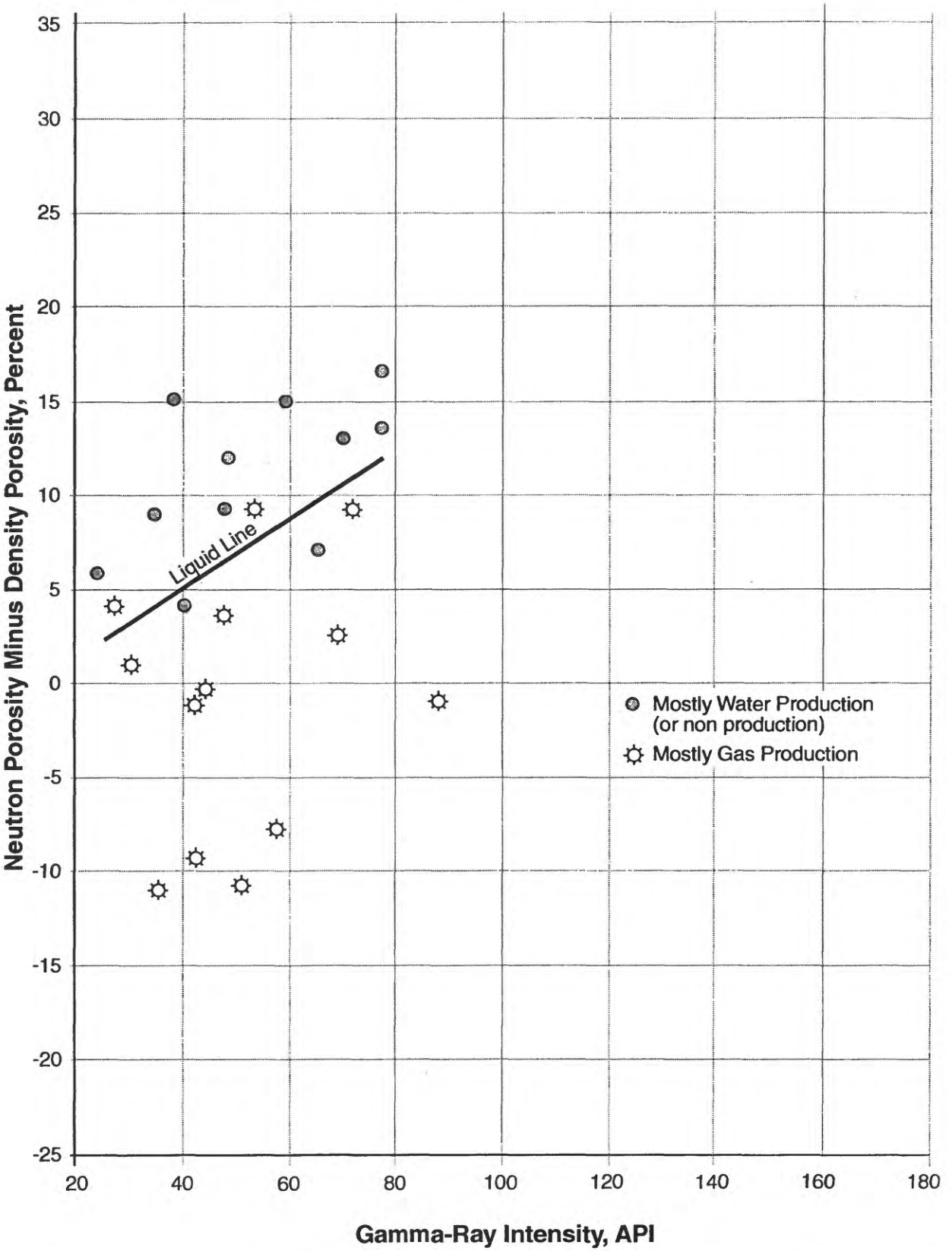

Figure 1. Crossplot of neutron porosity minus density porosity vs gamma-ray intensity showing hypothetical liquid line and producing-interval data.

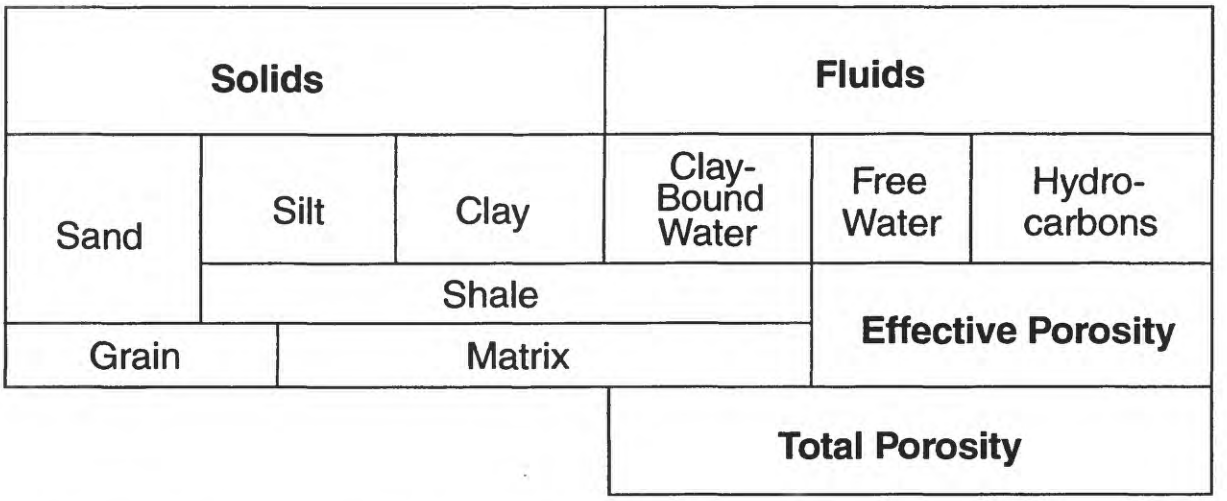

Figure 2. Generalized diagram illustrating schematic relation of solid and fluid portions of shaly formations using the dual water model (modified from Schlumberger, 1987).

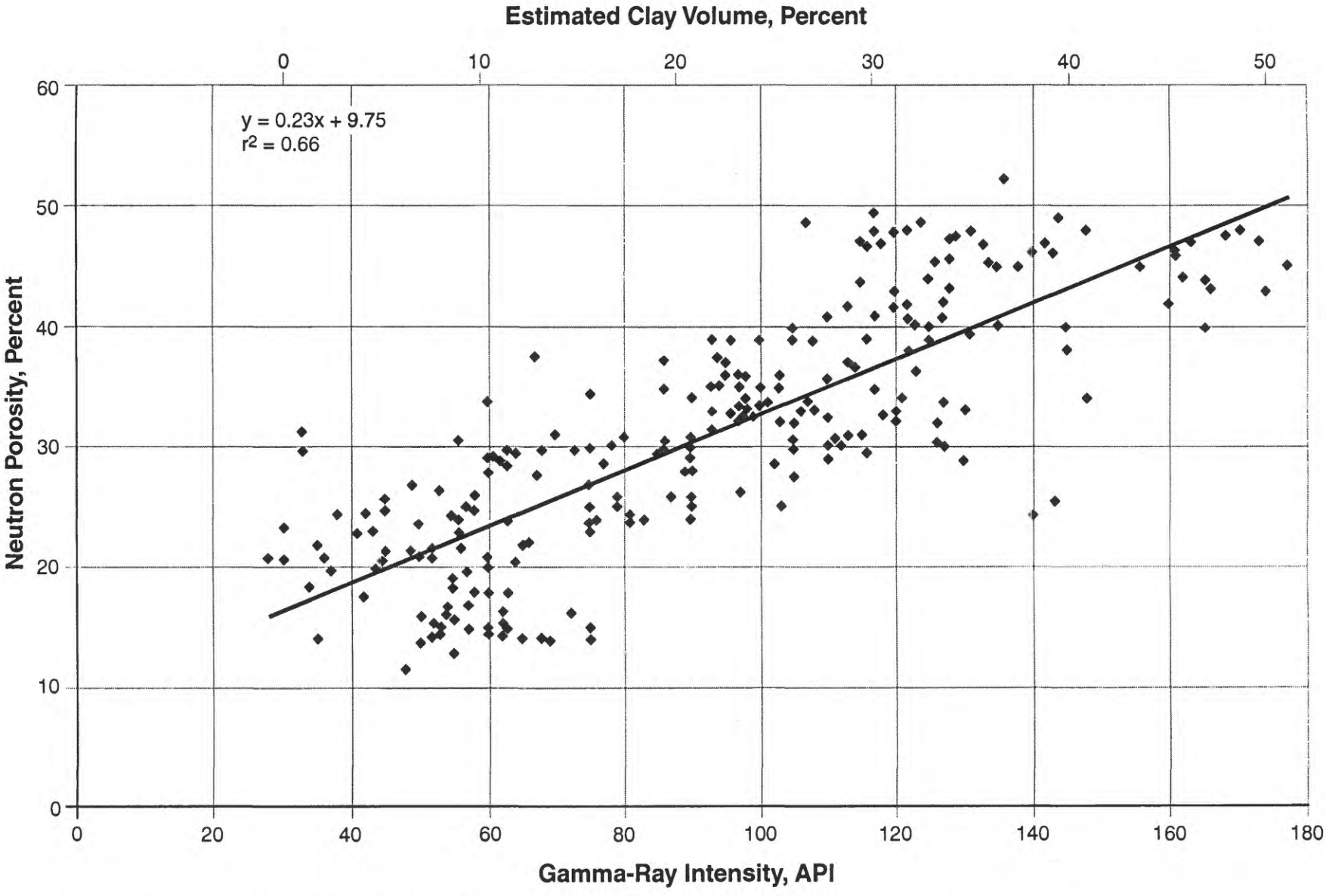

Figure 3. Crossplot of neutron porosity vs gamma-ray intensity for all gas-producing intervals of this report. Linear regression line shows average neutron response to bound water associated with clay. Data scatter reflects variations in effective porosity and gas saturation. Estimated clay volume is scaled opposite gamma-ray intensity (x-axis). Equation and sample coefficient of determination (r2) for regression line are shown in upper left.

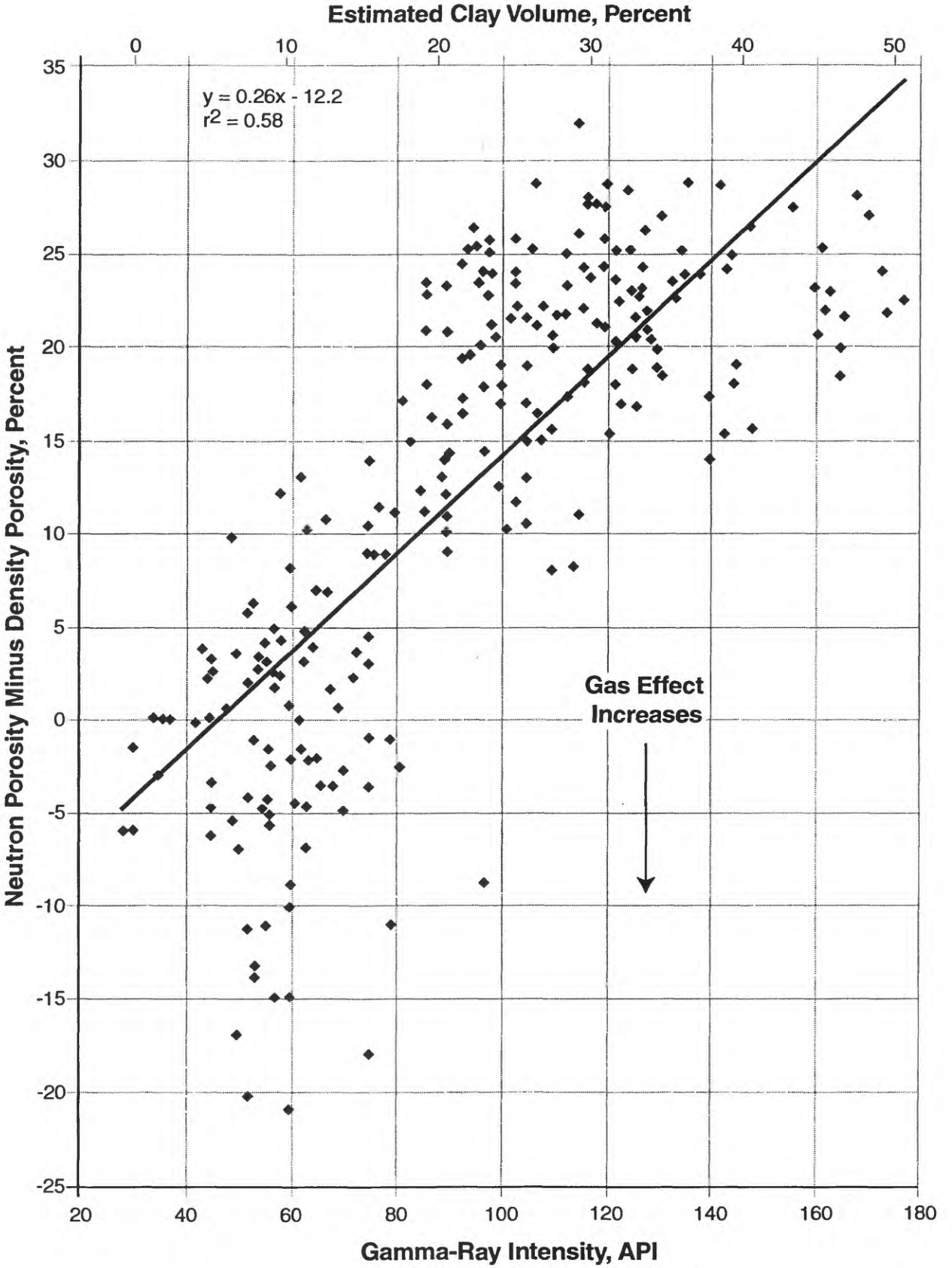

Figure 4. Crossplot of neutron porosity minus density porosity vs gamma-ray intensity for all gas-producing intervals of this report. Linear regression line shows average response of neutron porosity minus density porosity (N-D, y-axis) to bound water associated with clay. Data scatter reflects variations in the gas effect. Estimated clay volume is scaled opposite gamma-ray intensity (x-axis). Equation and sample coefficient of determination (r2) for regression line are shown in upper left.

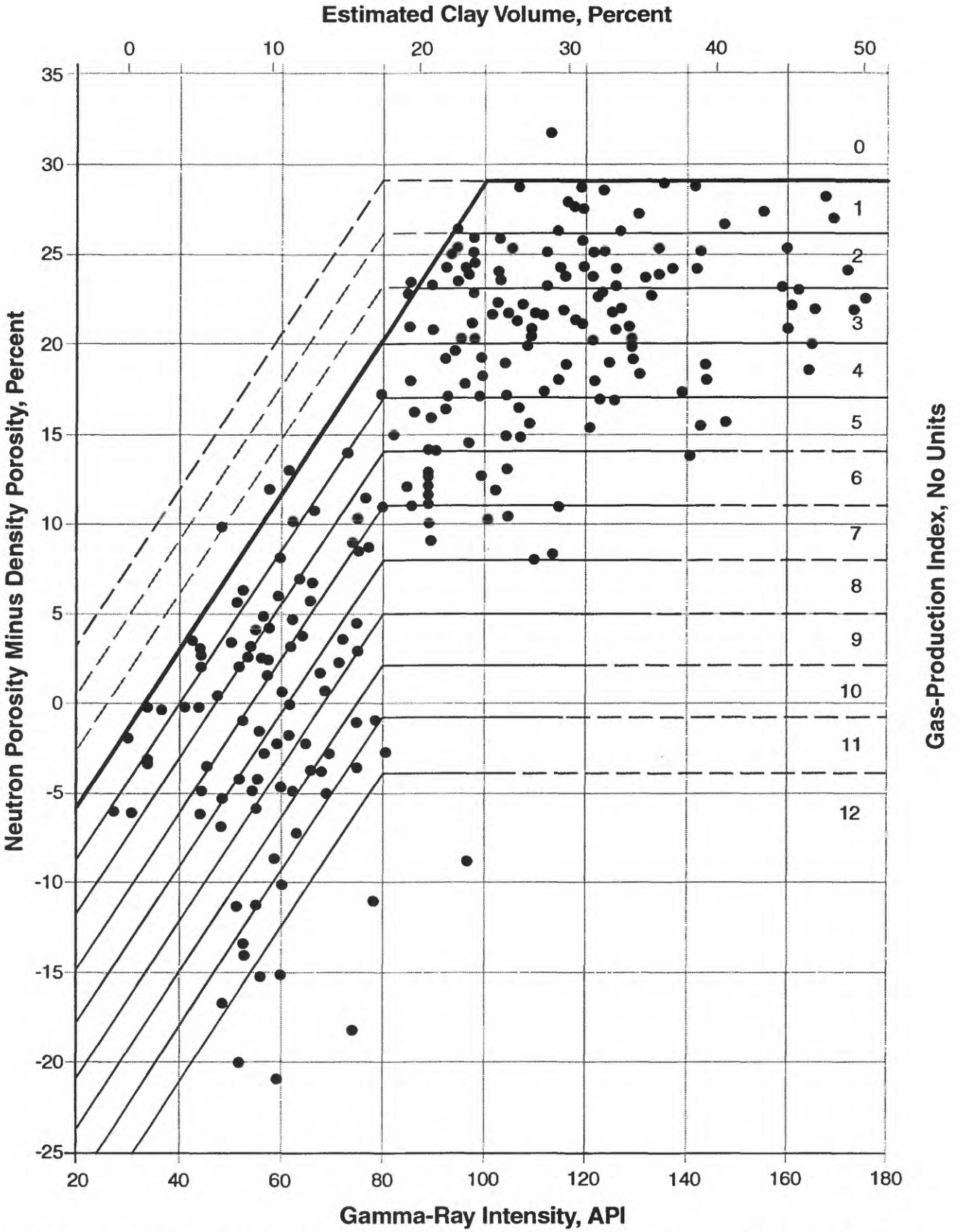

Figure 5. Crossplot of neutron porosity minus density porosity vs gamma-ray intensity for all gas-producing intervals of this report, combined with a calibration system composed of empirical (hand drawn) zero-production baseline (heavy diagonal and horizontal line segments) and 12 indexed levels of gas-production potential (thin diagonal and horizontal lines, dashed where inferred). Estimated clay volume is scaled opposite gamma-ray intensity (x-axis).

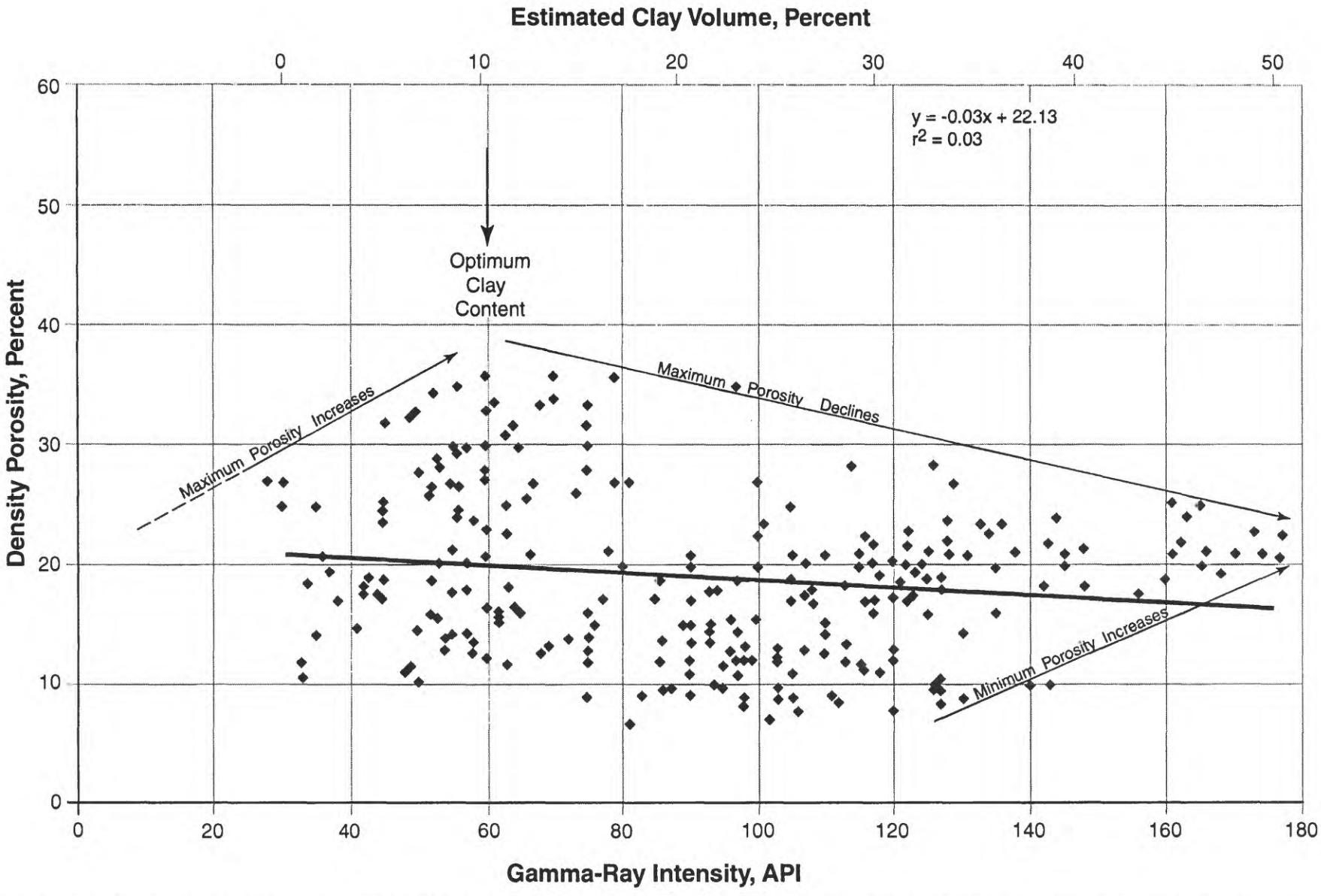

Figure 6. Crossplot of density porosity vs gamma-ray intensity for all gas-producing intervals in this report. Linear regression line (heavy solid line) shows average porosity of gas-producing intervals at a given clay volume. Estimated clay volume is scaled opposite gamma-ray intensity (x-axis). Equation and sample coefficient of determination (r2) for regression line are shown in upper right.

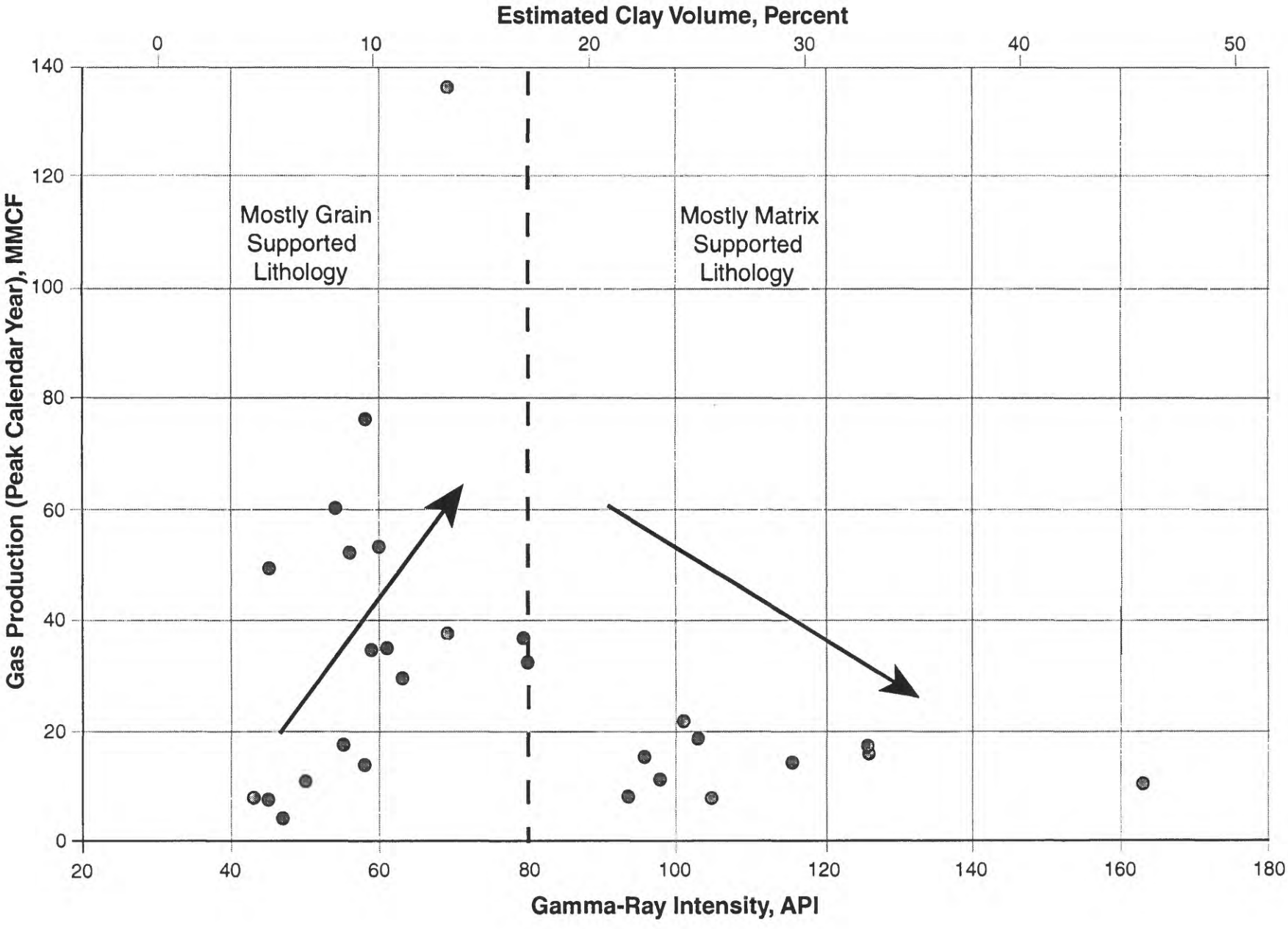

Figure 7. Crossplot of gas production in the peak calendar year vs gamma-ray intensity for 28 wells in northern Montana. Approximate transition (80 API) between mostly grain-supported and mostly matrix-supported lithologies is dashed. Gamma-ray intensity for each well is averaged from its constituent intervals (Figs. 3-6). Estimated clay volume is scaled opposite gamma-ray intensity (x-axis).

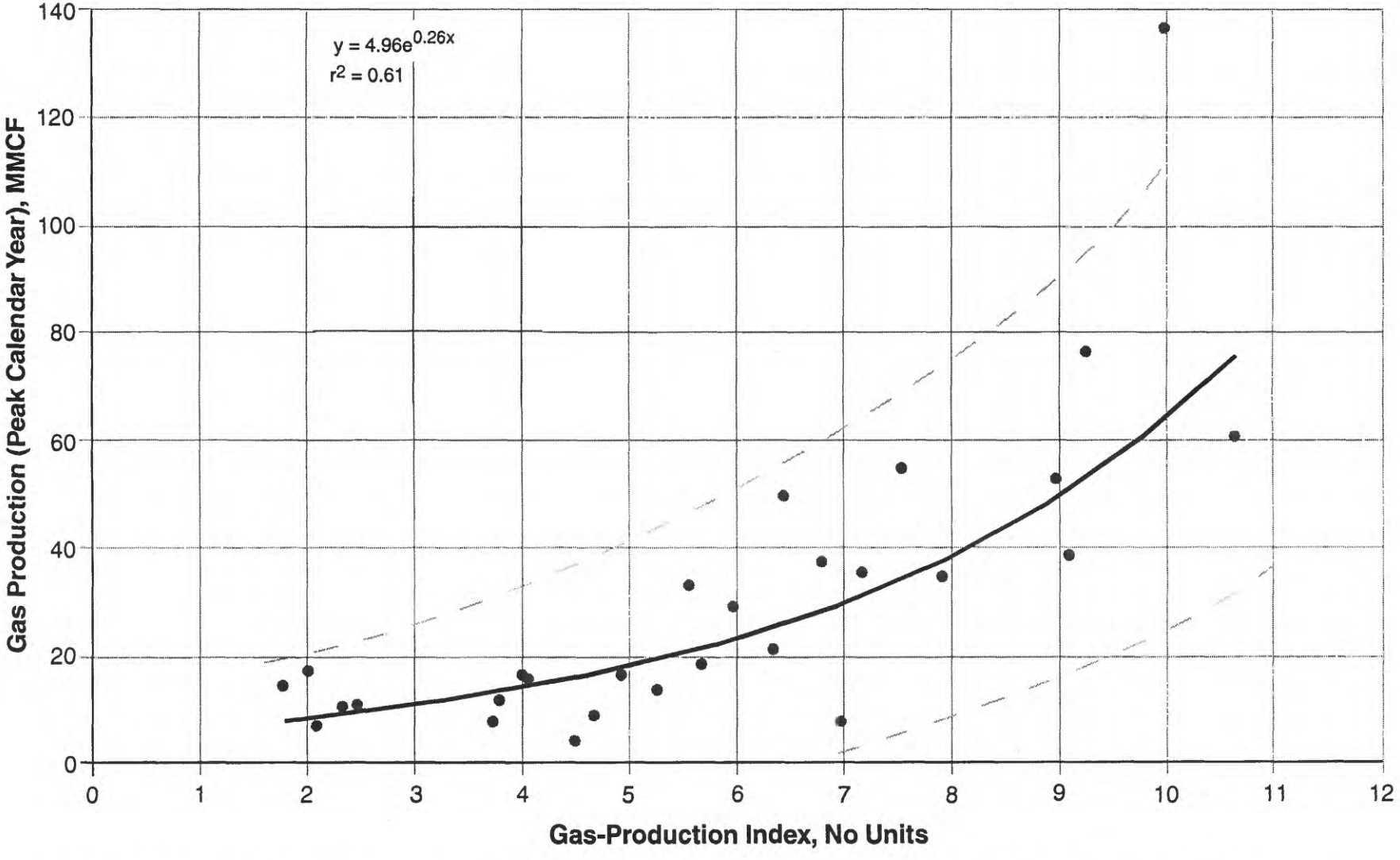

Figure 8. Crossplot of gas production in the peak calendar year vs gas-production index (from Fig. 5) for 28 wells in northern Montana. Dashed lines indicate approximate range of production associated with a given index level. Gas-production index for each well is averaged from its constituent intervals (Figs. 3-6). Equation and sample coefficient of determination (r2) for regression line are shown in upper left.

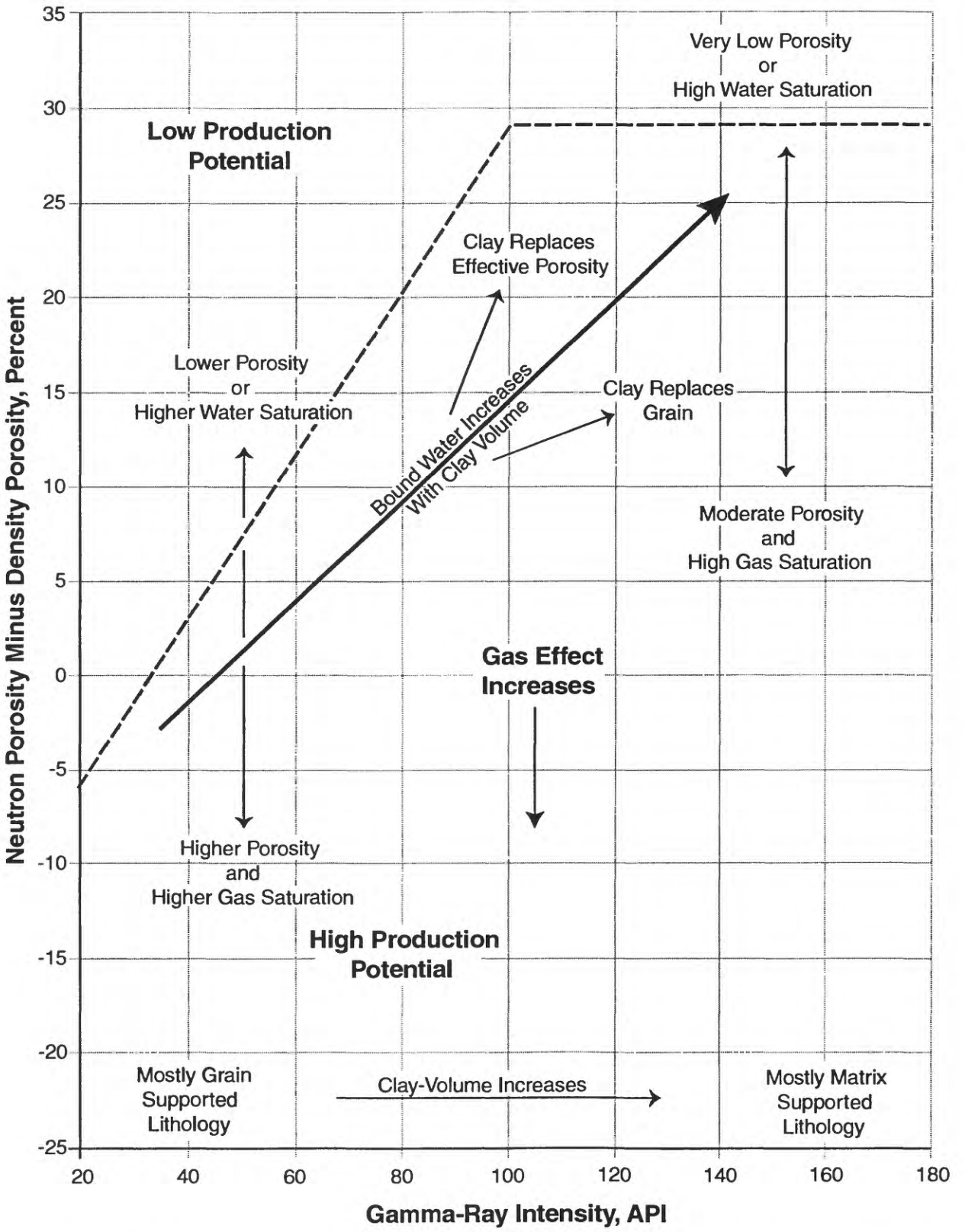

Figure 9. Summary crossplot of neutron porosity minus density porosity vs gamma-ray intensity, showing relative variation in porosity, water saturation, clay volume, bound water, and production potential, with plotted position of interval data. Heavy solid line is regression line of Figure 4. Dashed line is zero-production baseline of Figure 5.